Graphene oxide-mesoporous SiO2 hybrid composite for fast and efficient removal of organic cationic contaminants

Wlodzimierz Czepa, Dawid Pakulski, Samanta Witomska, Violetta Patroniak, Artur Ciesielski, Paolo Samori

Graphene oxide-mesoporous SiO_2 hybrid composite for fast and efficient removal of organic cationic contaminants

Włodzimierz Czepa[1,2,‡], *Dawid Pakulski*[1,2,3,‡], *Samanta Witomska*[1,2], *Violetta Patroniak*[1], *Artur Ciesielski*[3,*], *Paolo Samorì*[3,*]

[1] Faculty of Chemistry, Adam Mickiewicz University, Uniwersytetu Poznańskiego 8, 61614 Poznań, Poland.

[2] Center for Advanced Technologies Adam Mickiewicz University, Uniwersytetu Poznańskiego 10, 61614 Poznań, Poland.

[3] Université de Strasbourg, CNRS, ISIS 8 allée Gaspard Monge, 67000 Strasbourg, France.

‡ Those authors contributed equally to this work.

*Corresponding author. E-mail: ciesielski@unistra.fr , samori@unistra.fr

Abstract

In this study, we have developed a novel mesoporous SiO_2 - graphene oxide hybrid material (SiO_2NH_2-GO) as highly efficient adsorbent for removal of cationic organic dyes from water. The fabrication of such a three-dimensional (3D) SiO_2NH_2-GO composite has been achieved *via* the condensation reaction between the amine units exposed on 3-aminopropyl-functionalized silica nanoparticles and the epoxy groups on surface of GO. As a proof-of-concept, SiO_2NH_2-GO was used for the removal of archetypical dyes from water and revealed outstanding maximum adsorption capacity towards methylene blue (MB), rhodamine B (RhB) and methyl violet (MV) at pH 10 reaching 300, 358 and 178 mg g^{-1} for MB, RhB and MV, respectively, thus outperforming the neat components of composite, i.e. GO and SiO_2. Moreover, the adsorption process revealed that ~ 99.7 % of MB, RhB and MV have been removed in only 3 min thereby highlighting the superior nature of SiO_2NH_2-GO composite with respect to most of graphene oxide-based adsorbents of organic dyes. Finally, the composite was used in solid phase extraction (SPE) as column packing material, for continuous water purification, thus highlighting the great potential of SiO_2NH_2-GO for the large-scale removal of cationic dyes from aqueous solutions.

1. Introduction

The increasing contamination of aquatic systems with organic and inorganic pollutants represents a major challenge in the field of environmental science.[1] Since the dye manufacturing was introduced, more than 100 000 different water-soluble organic dyes are being used in a wide range of industries such as textile, paper, printing, leather, polymer, cosmetics and others.[2, 3] Noteworthy, organic dyes are considerably toxic for health and environment even in low concentrations,[4-6] and may cause cancerogenic and mutagenic effects, which can lead to health disorders such as dysfunction of the liver, brain and central nervous system.[5, 7, 8] It is well known that about 10-15 % of all dyes used in the industry are lost in the wastewater during processing. Therefore, the development of highly-efficient and low-cost purification methods is highly desirable.[9-11] Biodegradation of organic dyes is time-consuming and ineffective, therefore adsorbents with high (photo)chemical stability gained considerable attention in purification systems causing development of high performance and eco-friendly materials for adsorption.[12, 13] Among various dye removal techniques, adsorption process based on capturing the adsorbate (pollutants) by an adsorbent is attractive due to wide range of potential sorption materials with high efficiency and affinity toward miscellaneous contaminants.[14-16] Recently, atomically thin two-dimensional materials (2DMs) gathered a great interest in the scientific community due to their outstanding mechanical, electrical, optical and thermal properties, combined with a high chemical stability.[17] In particular, their highest surface-to-volume ratio endorses these materials as suitable candidates for the efficient adsorption of a wide range of contaminants.[18-21] On the other hand, 2DMs are insoluble and difficult to be dispersed in aqueous solutions due to their hydrophobic nature and tendency to aggregated in aqueous solution *via* strong van der Waals interactions. Moreover, their hydrophobic character also hampers the adsorption process of cationic dyes or heavy metal ions from aqueous solution on their surfaces. In this context, the adsorption capacity of 2DMs can be significantly increased by decorating them with functional

groups. Notably, its oxygen-containing functional groups such as epoxy, carbonyl and carboxylic moieties endows graphene oxide (GO) a multitude of facile functionalization possibilities as well as a good water dispersibility.[22-24] Because of these reasons, GO-based nanomaterials have been recently considered as attractive candidates for sequestering pollutants from aquatic systems[24, 25] in view of its superior features over the other adsorbents such as activated carbon. In fact the latter interacts with pollutants like water-soluble organic dyes *via* weak hydrophilic interactions, resulting in weak purification performance.[26] Moreover, oxygen containing groups of GO may undergo ionization or can act as electron acceptors, thereby allowing the occurrence of electrostatic interactions, π-π stacking and hydrogen bonding and eventually also ion exchange between dye molecules and surface of GO.[27, 28] Not surprisingly, it was reported that GO exhibits ultrahigh adsorption capacity towards cationic dyes and outperforms other adsorbents. In particular, the adsorption capacity of GO and its different forms including reduced GO (rGO), magnetic graphene oxide (MGO) and reduced magnetic graphene oxide (MrGO) was explored by Akrami *et. al.* [29] for adsorption of methylene blue (MB), which is one of the most widely used cationic dye. The maximum values of adsorption capacities were determined as 116 mg/g, 168 mg/g, 82 mg/g and 114 mg/g for GO, MGO, rGO and MrGO, respectively.[29] Yet, the high dispersibility of GO in water hampers its use in industrial systems since the residual GO cannot be easily removed from post-adsorption dispersions and may cause secondary pollution. To overcome this drawback, the functionalization of GO with organic and inorganic moieties have been explored which resulted in a large library of GO-based materials exhibiting strong adsorption affinity towards various pollutants.[28, 30-38] In this case, the fabrication of functionalized materials through covalent reactions between pristine GO nanosheets are particularly attractive. Noteworthy, the functionalization presented in this work aimed at generating a hybrid system in which synergistic effect between both components is one of the most important features of the newly obtained composite. Many different features affect this type of property, including specific

surface area, type of interactions between the components, mass transfer efficiency etc.[39] Another major limitation of neat GO arises from its poor porosity, which limits the number of available coordination sites. Such a problem can be potentially overcome by covalently bridging GO layers with molecular pillars to form three-dimensional (3D) macroscopic porous structures. On the other hand, mesoporous silica, introduced in the 1990s by Kresge,[40] is attracting a growing interest for water treatment chemistry due to its various remarkable properties such as high specific surface area, large pore size, chemical inertness. Depending on the morphological characteristics, presence of different functional groups and adsorption conditions, mesoporous silica might exhibit good adsorption efficiency towards organic pollutants. However, 3-aminopropyl-functionalizd silica itself exhibits relatively low adsorption capacity due to presence of partially protonated amine groups diminishing efficiency of cationic dyes electrostatic attraction. Yet, because of an abundant repertory of surface functional groups it can be chemically tailored for excellent selectivity towards specific contaminants, good stability and low-cost of production.[41-43] Several works exploring mesoporous silica and silica-modified functionalized with graphene oxide for applications have been reported, highlighting the potential of those hybrid materials in biomedicine, electrochemistry as well as efficient adsorption systems for heavy metal ions, organophosphorus pesticides and other organic contaminants.[44-50]

Here we report a facile and low-cost method to produce a novel generation of GO-based adsorbent obtained via the condensation between 3-aminopropylsilica particles (SiO_2NH_2) and GO for the effective removal of cationic dyes including methylene blue (MB), rhodamine B (RhB) and methyl violet (MV) from water (Figure 1). Different adsorption parameters were systematically investigated and a mechanism was proposed. The adsorption kinetics and isotherms of MB, RhB and MV cationic dyes on SiO_2NH_2-GO material were estimated with the pseudo-first and -second order as well as Freundlich and Langmuir isotherm model. Moreover, the SiO_2NH_2-GO hybrid was used as solid phase extraction (SPE) column packing

material which allows achieving high flow-rate with excellent recovery, precision and adsorption at the level of 99% of initial dye content.

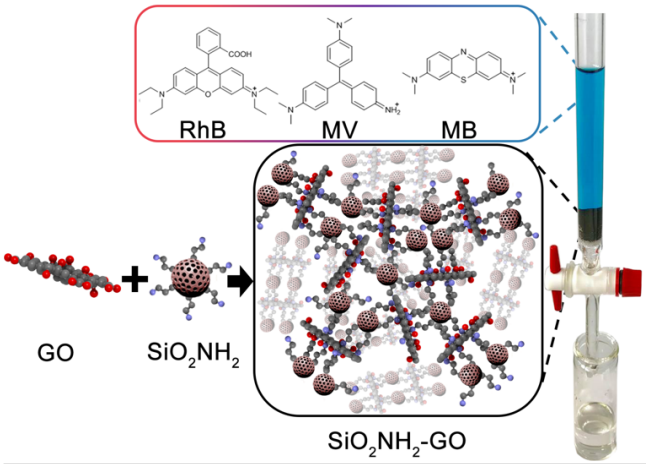

Figure 1. Chemical structures of the adsorbent (SiO_2NH_2-GO) and cationic dyes: methylene blue (MB) rhodamine B (RhB) and methyl violet (MV).

2. Experimental

2.1 Starting materials

Graphene oxide 4 mg mL^{-1} aqueous solution was acquired from Graphenea. 3-(aminopropyl)-functionalized silica (diameter of 40-63 µm), methylene blue, rhodamine B, methyl violet, ethanol, hydrochloric acid and sodium hydroxide were purchased from Sigma Aldrich and used directly without further purification. All the solutions were prepared using MiliQ DI water (0.05 µS cm^{-1}).

2.2 Preparation of SiO_2NH_2-GO adsorbent

A batch of SiO_2NH_2-GO is prepared as follows: a mixture of ethanol (50 ml) and GO (50 ml, 4 mg mL^{-1}) was sonicated for 15 min and then suspension of 3-(aminopropyl)-functionalized silica (1 g) dispersed in 200 ml of ethanol was added. The mixture was rigorously stirred overnight under reflux. The precipitate was then filtrated and rinsed with a large amount of water and ethanol. The resulting black powder was then freeze-dried for 24h under vacuum.

2.3 Characterization

The morphology of SiO_2NH_2-GO was analyzed by scanning electron microscopy (SEM) with a FEI Quanta 250 FEG instrument equipped for energy dispersive X-ray (EDX) analyses. The accelerating voltage was 5 keV incident beam energy. SEM samples were placed on alumina substrates. X-ray powder diffraction (XRD) experiments were conducted on powder specimens using Bruker ASX D8 Advanced equipped with Cu anode with Kα radiation (λ = 1.5418 Å). Diffraction patterns were collected at room temperature in the scattered angular range between 6° and 40° with an angular resolution of 0.02° per step and a typical counting time 4 of 10 s per step. Fourier transform infrared (FTIR) spectra of samples were recorded on Perkin Elmer Spectrometer (Spectrum Two) equipped with ATR Diamond in the range of 400-4000 cm^{-1}. The specific surface areas were measured by means of a Micromeritics ASAP 2050 surface area and porosity analyzer. The specific surface area was calculated from adsorption/desorption isotherms of N_2 at 77 K by multi-point Brunauer–Emmett–Teller (BET) method. The pore size distribution was obtained from Barret−Joyner−Halenda (BJH) method. The samples were previously outgassed for 10 hours at 100 °C. X-ray photoelectron spectroscopy (XPS) analyses were carried out on a Thermo Scientific KAlpha X-ray photoelectron spectrometer with a basic chamber pressure of ~10^{-9} mbar and an Al anode as the X-ray source (X-ray radiation of 1486 eV). Spot sizes of 400 µm were used and pass energies of 200.00 eV for wide energy scans and 10.00-20.00 eV for scans were used. 5 mg of GO, SiO_2NH_2 and SiO_2NH_2-GO were attached to copper film. Thermal gravimetric analysis (TGA) decomposition curves are recorded in the range 25-700°C operating under nitrogen atmosphere, with a thermal step of 10 °C/min on a Mettler Toledo TGA/SDTA851e system. Raman spectra were recorded by a Renishaw microscope with a 100× objective, laser excitation wavelength of 532 nm and laser power of 0.05%. The silicon peak at 520.3 cm^{-1} was took as reference for wavenumber calibration. Point of zero charge of adsorbent was determined following previously reported method.[51] The

concentration of samples was evaluated using UV-Vis spectra observing adsorption at 664, 554, 579 nm for methylene blue, rhodamine B and methyl violet, respectively.

2.4 Adsorption studies

The maximum adsorption capacity (q_{max}) was investigated by adsorption isotherms representing the mathematical relation of the organic dye adsorbed by one gram of adsorbent to the equilibrium solution concentration at constant temperature.[52] The adsorption of organic dyes on SiO_2NH_2-GO was carried out by mixing 5 mg of adsorbent and 15 ml of dye solution at the desired concentration, then solution pH was adjusted with HCl (0.1 M) or NaOH (0.1 M) to study the effect of initial pH. The mixtures then were stirred with speed of 400 rpm for 24 hours at room temperature to achieve the adsorption equilibrium. The adsorbent was separated from the dye solution by centrifugation and the equilibrium concentration of the dye in solution was determined by means of UV-Vis spectroscopy. The adsorption capacity q (mg g^{-1}) of dyes onto SiO_2NH_2-GO hybrid was calculated from the following equation:

$$q = \frac{(C_0 - C_e)V}{m_{ads}}$$

Where q (mg g^{-1}) is amount of organic dye adsorbed on SiO_2NH_2-GO at equilibrium, C_0 and C_e are the initial and equilibrium concentrations of dyes in solutions (mg L^{-1}) respectively, V is the volume of solution (L) and m_{ads} is mass of adsorbent used (g). Among various adsorption isotherm models Freundlich and Langmuir are most commonly used for the analysis of organic dyes adsorption. The Freundlich model can be expressed as[16, 52]:

$$q_e = K_F C_e^{1/n}$$

where K_F (L mg^{-1}) and 1/n are the Freundlich adsorption constant, representing adsorption capacity, and adsorption intensity, respectively. C_e represents equilibrium concentration of organic dye while q_e is amount of dye adsorbed at equilibrium time. The Langmuir is represented by following equation:

$$q_e = \frac{q_{max} K_L C_e}{1 + (K_L C_e)}$$

where C_e and q_e are as defined above, q_{max} (mg g^{-1}) and K_L (L mg^{-1}) are Langmuir adsorption constants related to adsorption capacity and adsorption rate, respectively.

2.5 Kinetics and thermodynamics

In the present study, the kinetics of an adsorption process are investigated using the pseudo-first and pseudo-second order rate adsorption models were performed at 298, 303, and 313 K under the conditions of pH 10 by mixing 30 mg of adsorbent into 50 ml (conc. 50 mg L^{-1}) of MB, RhB and MV at 25°C at pH of 7. The pseudo-second-order rate equation of McKay and Ho can be represented as:

$$\frac{t}{q_t} = \frac{1}{k_2 q_e^2} + \frac{t}{q_e}$$

where q_e, q_t and t are defined above, k_2 represents rate constant (g min^{-1} mg^{-1}).

The thermodynamics of the adsorption process was investigated by using the aforementioned conditions at three different temperatures: 298, 313 and 333 K. The free energy changes of the sorption reaction are given by the following equation:

$$\Delta G^0 = -RTlnK_d$$

where ΔG° represents standard Gibbs free energy change, R is the ideal gas constant (8.314 J $mol^{-1}K^{-1}$), T is the absolute temperature (K) and K_d is the distribution coefficient. The enthalpy ΔH^o and the entropy ΔS^o changes can be calculated from the van't Hoff equation:

$$lnK_D = \frac{\Delta H^0}{RT} + \frac{\Delta S^0}{R}$$

2.6 Solid Phase Extraction (SPE) experiments

The SPE purification column was prepared by placing 2 g of SiO_2NH_2-GO suspended in distilled water inside of glass column with diameter of 30 mm and lower frits of 5 µm. Column filling was firstly activated using NaOH solution (100 mL, 0.1 M). Adsorption experiments

were carried out by passing one liter of each organic dye (50 mg L^{-1}) through SPE column and then determined by UV-Vis spectroscopy. In order to re-generate SPE column, 1 M HCl followed by Millipore deionized water was passed through the column. The adsorption capacity variation upon SiO_2NH_2-GO regeneration is defined as: $(q/q_{max}) \times 100$, where q_{max} is maximum adsorption capacity.

3. Results and Discussion

3.1. Synthesis and Characteristics of SiO_2NH_2-GO

In order to understand the nature of the interaction between the SiO_2NH_2 and GO, a comprehensive physical and chemical analysis was performed. Scanning electron microscopy (SEM) was employed to study the morphology of the multicomponent systems. The images in Figure 2c show that SiO_2NH_2-GO exhibits a homogenous porous structure with respect to pristine SiO_2NH_2 and GO (Fig. 2a-b). Energy-dispersive X-ray spectroscopy (EDX) investigation (Figure 2b) provided evidence for the uniform distribution of the SiO_2NH_2 particles within the hybrid SiO_2NH_2-GO material.

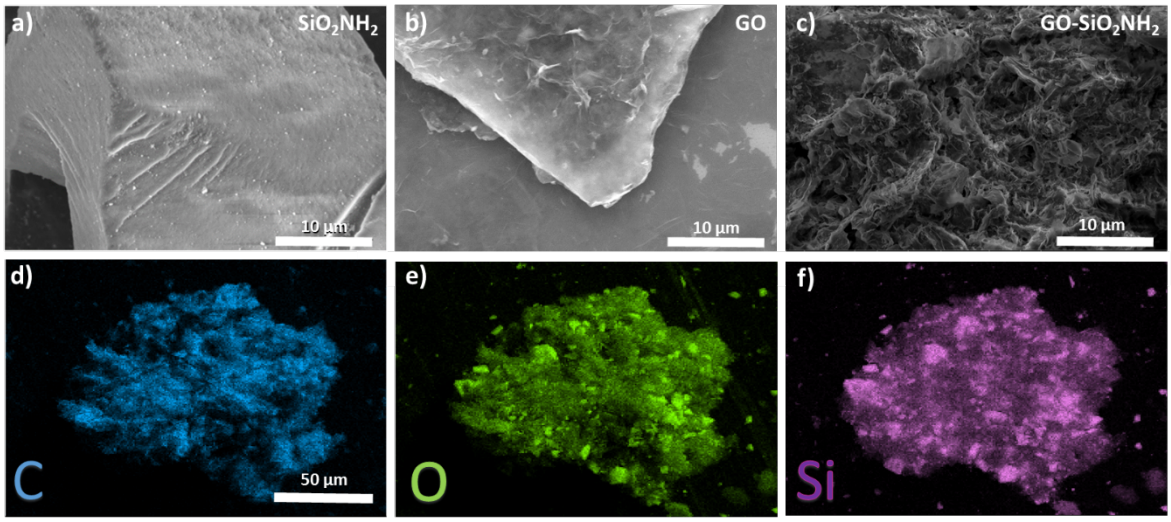

Figure 2. Scanning electron microscopy (SEM) image displaying the morphology of a) SiO_2NH_2 b) GO and c) SiO_2NH_2-GO and EDX elemental mapping of d) carbon (C, blue), e) oxygen (O, green) f) silicon (Si, purple).

The porosity of SiO_2NH_2-GO was investigated by adsorption-desorption isotherms of N_2 at 77 K. It revealed a specific surface area, as calculated by Brunauer-Emmett-Teller (BET) model, of 405.5 m^2g^{-1}. Such value is much greater than the one quantified in the starting GO material which displays a specific surface area of ca. 108 m^2 g^{-1}. The increase is provided by attachment of GO sheets to the SiO_2NH_2 with large specific surface area (341.8 m^2 g^{-1}), which can be also observed on XRD spectra as significant increase in the inter sheets spacing (Figure 3a). The average pore size diameter, as calculated with the Barrett-Joyner-Halenda (BJH) model, amounts to 70.4 Å (see Table S1 in Supporting Information). Fourier transform infrared spectroscopy (FTIR) was used to prove the covalent cross-linkage of the SiO_2NH_2 particles to GO (Figure 3b). The pristine GO displays typical peaks corresponding to a variety of oxygen-containing functional groups. The peak at 1724 cm^{-1} is attributed to the C=O stretching of carboxylic acid groups, 1624 cm^{-1} to the sp^2 C=C bonds, 1216 cm^{-1} and 1054 cm^{-1} to C–O stretching of epoxy and alkoxy groups, respectively and a broad band due to O–H stretching vibrations in carboxyl and alcohol functionalities around 3390 cm^{-1}.[53] The spectra of SiO_2NH_2 exhibit very strong and broad band at 1075 cm^{-1} which is usually assigned to the Si-O-Si asymmetric stretching vibrations, whereas the band at 801 cm^{-1} corresponds to Si-O-Si symmetric stretching vibrations. Once the aminosilica interacts with GO, a reaction between amine groups of SiO_2NH_2 with epoxy units located on the basal plane of GO flakes takes place. As a result, the reaction is accompanied by a strong decrease in the intensity of the C-O band with the appearance of strong and broad absorption at 1075 and 801 cm^{-1}, which was not monitored in the neat GO and corresponds to Si-O-Si bond from SiO_2NH_2 material. Such a result confirmed the structural integrity of SiO_2NH_2 whose architecture is well retained in the hybrid structures SiO_2NH_2-GO. Moreover, the shift of peak at 1631 cm^{-1} visible on SiO_2NH_2 spectra which corresponds to N-H bending of primary amines shifts to 1670 cm^{-1} confirming formation of secondary amine group while functionalization. The significant decrease of peak intensity at 1724 cm^{-1}, compared to the spectra of pristine GO and SiO_2NH_2-GO, suggests the

partial reduction of carbonyl species, which takes place during the functionalization process. The SiO_2NH_2-GO hybrid was further characterized by Raman spectroscopy which is a well-established technique to explore carbonaceous materials. Raman spectra (see Figure S1) exhibit two prominent peaks of GO, i.e. the D band (1358 cm^{-1}) corresponding to sp^3-hybridized carbon atoms and the G band (1592 cm^{-1}) originated from the scattering of the E_{2G} photon of the sp^2-hybrydized carbon bond from the aromatic regions of GO.[54, 55] Comparably, in spectrum of SiO_2NH_2-GO the value of G band shifts to a lower wavenumber, reaching 1586 cm^{-1}, thereby confirming the covalent functionalization of the graphitic materials.[56] Typically, chemical modification of graphene materials is often characterized by the changes in the ratio of the D and G bands areas. The intensity ratio I_D/I_G is commonly used to determine the degree of functionalization of graphene-based nanostructures.[57] As the result of the functionalization, the I_D/I_G intensity ratio increases from 0.93 to 1.12, offering an indirect evidence of the increased content in sp^3 carbon atoms upon functionalization. The crystallinity, and in particular the interlayer distance within GO and SiO_2NH_2-GO were investigated by wide-angle X-ray scattering (WAXS) (Figure 3c). A typical sharp peak 2θ at ~10.01° for pristine GO corresponds to an interlayer spacing of 0.87 nm due to the (002) reflection of stacked GO sheets, in accordance with previously reported values.[58, 59] Additionally, an amorphous peak at 2θ = 22.15° was recorded and corresponds to silica particles characterized by variable Si-O-Si bond angles. Upon functionalization process, the typical 2θ peak of GO (distance 1.06 nm) shifts toward lower angles 2θ = 8.35°, which can be assigned to solvent molecules intercalation. Moreover, the high intensity of broad peak coming from amorphous content provides evidence for the presence of a significant amount of silica in the SiO_2NH_2-GO hybrid material. The thermal stability of GO, SiO_2NH_2 and SiO_2NH_2-GO was investigated by means of thermal gravimetric analysis (TGA). Figure S2 reveals that GO undergoes a significant weight loss (ca. 40%) in the range of 150-300°C, likewise the SiO_2NH_2-GO composite, indicating the decomposition of oxygen-containing functional groups.[60] Notably, SiO_2NH_2 exhibits high

thermal stability showing a minor weight loss starting at 350°C caused by organic content decomposition, which is also observed for the SiO_2NH_2-GO hybrid. High-resolution X-ray photoelectron spectroscopy (XPS) measurements of pristine GO and SiO_2NH_2-GO made it possible to gain further information onto the chemical composition of materials (Figure 3d-f). The significant difference between the carbon (C1s), oxygen (O1s) and nitrogen (N1s) peaks provided evidence for the chemical bond formation between the oxygen-containing functional groups on the surface of GO and amine groups from SiO_2NH_2. In particular, wide energy spectrum exhibited the appearance of new peaks in SiO_2NH_2-GO hybrid material at 400.4 eV, 144.6 eV and 102.0 eV corresponding to N1s, Si2s and Si2p signals, respectively (Figure S3). The C1s XPS spectrum of the neat GO (Figure 3d) shows typical peaks at 284.5 eV (C-C/C=C), 287.8 eV (C-O), 286.6 eV (C=O) and 288.6 eV corresponding to carboxylic species present on edges of GO. Comparably, the C1s spectra of SiO_2NH_2-GO feature a new prominent peak at 286.0 eV, which can be assigned to C-N bonds present in amino silica and also resulting from the reaction of amine groups with opening epoxy rings (Figure 3f). Moreover, a significant decrease of peak corresponding do C-O moieties suggests major functionalization due to epoxide ring opening. In parallel to the functionalization reaction, a slight reduction of carbonyl functional groups on GO surface is observed on C1s spectra, which is in the line with FTIR results. The high resolution O1s spectrum of SiO_2NH_2-GO indicates the presence of both Si-O and C-O peaks at 532.2 eV and 533.5 eV, respectively also existing in O1s spectra of GO and SiO_2NH_2 solely (Figure S4a-c). Moreover, changes due to the introduction of nitrogen species within the GO structure are observed in the high-resolution N1s spectra indicating the successful functionalization of SiO_2NH_2 with the GO nanosheets (Figure S4d-f). The N1s spectrum of SiO_2NH_2 can be deconvoluted into three main peaks at 399.0 eV and 401.5 eV and 402.5 eV which can be ascribed to residual primary amines, secondary amines created while opening of epoxides and quaternary amines (NH_4^+) which co-participate in functionalization providing electrostatic interactions with deprotonated carboxylic species. Notably, the amount

of N-C bonds increases due to reaction between NH_2 groups of silica with epoxy-carbon atoms on surface of GO.

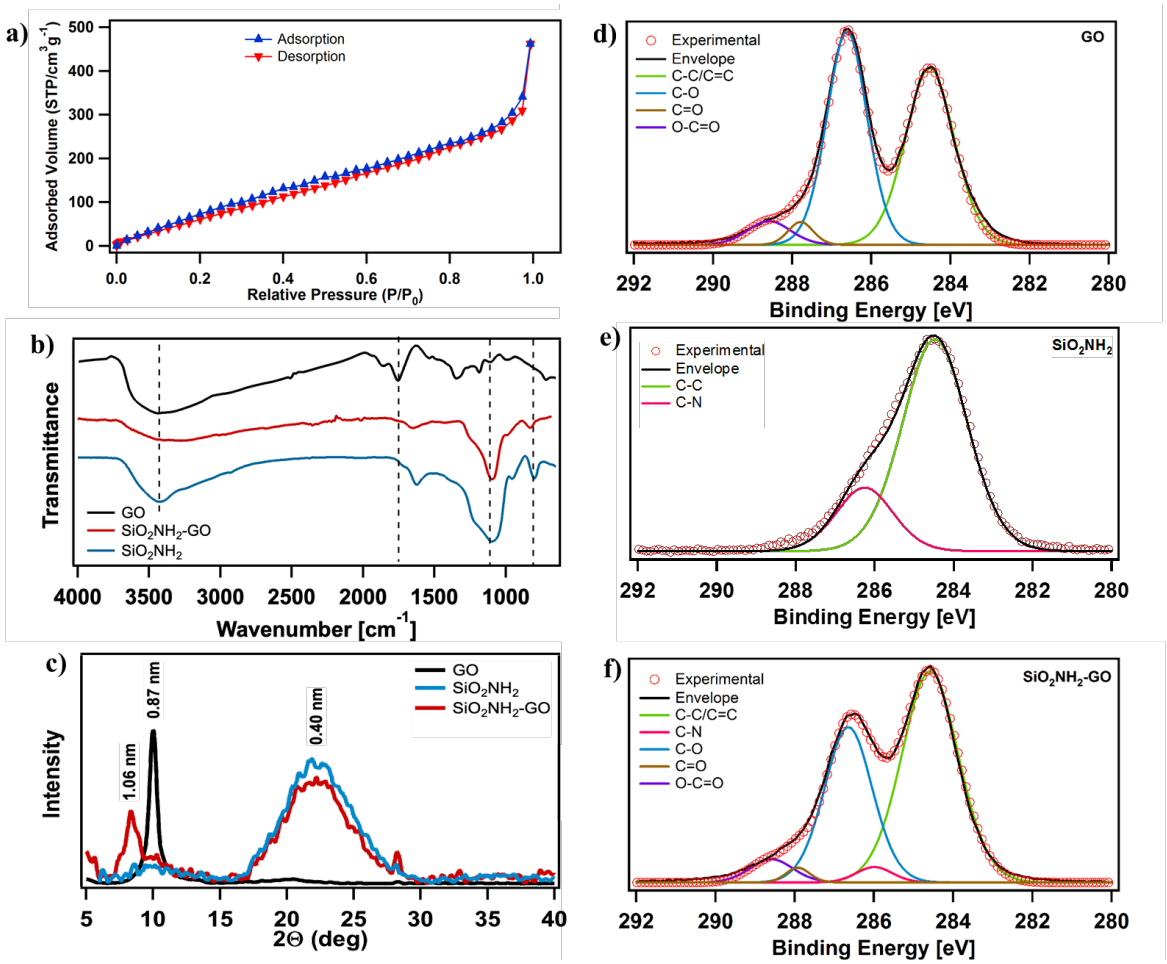

Figure 3. (a) BET adsorption/desorption isotherm of N_2 for SiO_2NH_2-GO composite. (b) FTIR spectra of GO, SiO_2NH_2 and SiO_2NH_2-GO composite. (c) XRD patterns of GO, SiO_2NH_2 and SiO_2NH_2-GO composite. C1s high-resolution XPS spectra of: (d) GO, (e) SiO_2NH_2 and (f) SiO_2NH_2-GO.

Zeta potential measurements done in aqueous solutions of GO and SiO_2NH_2 samples in function of pH (Fig. S14) provide important insight into the dispersion stability of colloids and electrostatic interaction between different graphene oxide sheets. The obtained results reveal that, the zeta potential of GO is highly negatively charged with an average value of -35 mV at pH over 4, which are resulting from the presence of the oxygen species its surfaces. It is evident from the literature that a zeta potential absolute value of higher than 30 mV indicate the stability of the graphene oxide suspensions.[61] On the other hand, the SiO_2NH_2 is negative surface charged when pH value is above 8 and the negative charge density increases with the increasing

pH. The zero point of zeta potential for SiO_2NH_2 is reached at pH 8.3 due to the protonation of amine groups on the surfaces. As a result, the deprotonated surface of SiO_2NH_2 favors the adsorption of cationic species by electrostatic attraction in a pH range of 10-12.

3.2. Adsorption of organic dyes on SiO_2NH_2-GO

To investigate the superior adsorption capacity of the SiO_2NH_2-GO, batch tests of the adsorption performance of SiO_2NH_2, GO and SiO_2NH_2-GO were conducted. Three prototypical water-soluble cationic dyes were chosen, i.e. methylene blue (MB), rhodamine B (RhB) and methyl violet (MV). Q_{max} and additional parameters obtained from Langmuir and Freundlich isotherm models are summarized in Tables S2. The Freundlich isotherm can be employed to describe heterogonous surfaces and multilayer adsorption system, while the Langmuir model can be assigned for the assumption of monolayer adsorption excluding interactions between adsorbed molecules. For the sake of comparison, control experiments, in which starting materials of GO or SiO_2NH_2 are used as adsorbents, are also carried out (see Table S3 and Figures S5-S6). Noteworthy, the adsorption isotherms of organic dyes on SiO_2NH_2-GO composite are fitted better by Langmuir model than by the Freundlich, suggesting the majority of monolayer coverage (Figure 4a-c). However due to the complexity of adsorption process, both mechanisms might occur simultaneously. The maximum adsorption capacities at pH 10 are 300 mg g^{-1} for MB, 358 mg g^{-1} for RhB and 178 mg g^{-1} in case of MV. Notably, the obtained values are almost three times greater than in case of adsorption on GO itself and several times higher than values obtained for SiO_2NH_2. The q_{max} values expressed in mmol g^{-1} amount to 0.97, 0.79 and 0.42 for MB, RhB and MV, respectively, implying that 1 g of SiO_2NH_2-GO can adsorb from approx. 0.5 to 1 mmol of cationic dyes from aqueous solutions. These values can be considered as very promising for the sorbents of cationic dyes compared to the previously reported chemically modified graphene materials (see Table S4 in Supporting Information). Noteworthy, while the overall charge of investigated dyes is nearly identical, the maximum

adsorption capacity expressed in mmol g^{-1} revealed the significant difference between MB, RhB and MV. In general, carbonaceous materials such as CNTs[62] or activated carbons[63] show the highest adsorption for MB, medium values for MV and the lowest adsorption for RhB. This variation is commonly attributed to the dye molecular size. For the larger dye molecules, adsorption can only occur at surface and it is difficult for the dyes to enter into the inner smaller pores of carbons. Such dye adsorption behavior is notably different for SiO_2NH_2-GO, where the maximum adsorption capacity of three dyes follows the trend MB > RhB > MV.

Noteworthy, although in general the functionalization of GO results in formation of highly porous structures, the pore sizes of such systems are rather low. This trend is also reflected in the present case where the large surface area (405.5 m^2 g^{-1}) is accompanied by pore size of diameter of around 70 Å, which limits the accessible area for large dyes (RhB) penetration. On the other hand, the adsorption capacity of RhB on the SiO_2NH_2-GO surface is supplemented by the strong electrostatic interaction resulting from the presence of both positive and negative charges in RhB structure. Furthermore, the pKa values for MB, RhB and MV are 3.8, 3.7 and 9.4, respectively.[64, 65] As the maximum adsorption was investigated at pH 10, MB and RhB are completely deprotonated at this conditions while MV might occur residual protonated groups which results in its lower adsorption capability.

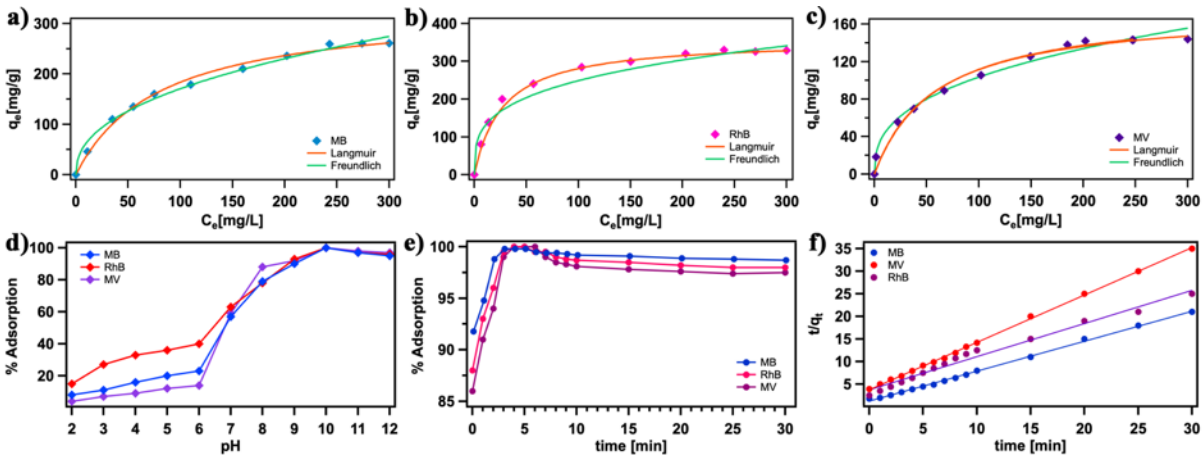

Figure 4. Uptake of organic dyes as the function of initial concentration of (a) methylene blue (MB) (b) rhodamine B (RhB) and (c) methyl violet (MV). The uptake experiments were carried out at pH=10 (stirring speed 400 rpm, t=24h). (d) Experiments conducted at different pH values.

(e) Time dependent organic dyes sorption on SiO_2NH_2-GO material (C_0= 50 mg g^{-1} T= 25 °C, stirring speed = 300 rpm, pH = 7). (f) The kinetic plots obtained by pseudo-second order model reactions.

3.3. Adsorption mechanism

It is well known that different factors involving structure and functional behavior of adsorbate impact on the dye adsorption mechanism. Among them, pH is well-known to affect the structure of adsorbent as well as the final form of compound used in adsorption process.[35, 66, 67] To gain further insight into the adsorption process, the effect of solution pH, initial dye concentration and contact time were examined. In general, GO-based materials exhibit higher adsorption capabilities towards cationic dyes at higher pH values.[29] In particular, above pH_{pzc} when the surface of GO is negatively charged the adsorption of cationic molecules is favored. The increase of negative charge on GO surface occurs as a consequence of carboxylic and hydroxide species deprotonation at pH > pH_{pzc}. Thus, the maximum adsorption values of organic dyes on GO are observed at pH > 3.9 and remain similar when the pH of solution is increased up to 12 (Figure S12). Similar tendency is observed for aminosilica as the deprotonation of amine groups and well known dissociation of silanol groups take place,[68] and leads to the generation of negative charges resulting in the higher adsorption efficiency with the increase of pH (Figure S12). The effect of pH on the adsorption of MB, RhB and MV on SiO_2NH_2-GO hybrid material was investigated at pH range from 2 to 12. The adsorption capabilities of SiO_2NH_2-GO at different pH are presented in Figure 4d. Notably, low pH conditions (2-6) result in low adsorption capability as only approx. 20% for MB and MV and less than 35% for RhB of the initial dyes were removed at pH 4. At pH 7, which corresponds to point of zero charge of SiO_2NH_2-GO, a further increase in the adsorption efficiency is observed. Further experiments revealed a maximum adsorption capacity of 99.7% relative to initial dyes content at pH = 10. Alongside the electrostatic interactions, which rule the adsorption mechanism, the planar structure of GO sheets favors the presence of π-π interactions.

In the present case organic dyes act as π-electron acceptors of residual π-electron rich regions of GO enhancing the adsorption of dyes as previously reported for graphene based nanostructures.[69, 70]

On the other hand, we have used FTIR to monitor the interaction between dyes and SiO_2NH_2-GO in the solution (Figure S7). The spectra recorded after adsorption of dye displayed a significant increase of the peak at 3418 cm^{-1} which can be attributed to presence of hydrogen bonds and indicates that such interactions might be also important in organic dyes adsorption. Moreover, after adsorption of MB there is a slight shift from 1607 to 1601 cm^{-1} corresponding to C=C bonds and the existence of confirming π-π interactions. Unfortunately, understanding the exact adsorption mechanism is a more complicated task, which goes beyond the scope of this work. However, it is fair to conclude that the aforementioned results suggest that tested cationic dyes can be easily adsorbed via electrostatic interactions and this type of interactions play a significant role in the adsorption of MB, RhB and MV onto the surface of SiO_2NH_2-GO. In accordance with the abovementioned analyses, we may conclude that size and large specific surface area of silica particles facilitates homogenous distribution of GO on SiO_2 limiting the aggregation of components themselves. Ultimately, the combination of GO and SiO_2NH_2 allows formation of hybrid composite with enhanced adsorption performance towards cationic dyes.

3.4. Kinetics and Thermodynamics of Adsorption

A kinetic investigation of the adsorption process can be accomplished by evaluating the rate and mechanism of mass transfer of adsorbate from liquid phase to solid adsorbent surface. The time required to reach equilibrium is an important parameter for dye removal. The pseudo-second-order kinetics model has been extensively used to predict dye adsorption kinetics.[71] It reveals that the adsorption displays a remarkable increase at the beginning of the experiments and then it reaches a plateau. Figure 4e shows that the initial rate of cationic dyes adsorption

increased sharply with time and reached a maximum ~99.7% within 3 min, and then it reaches a plateau. When the initially fast adsorption process is over, the dyes adsorption kinetic rate was adjusted by mass transport in the composite material.[72, 73] The experimental values of adsorption capacity and linear regression coefficient showed that the adsorption of cationic dyes is better fitted by pseudo-second order kinetics (Figures 4f) than pseudo first order kinetics (Figure S8), indicating that the adsorption process is driven by the strong surface complexation of cationic dyes with the oxygen and nitrogen containing groups of SiO_2NH_2-GO. The calculated kinetic parameters for adsorption of MB, RhB and MV dyes at pH 10 are listed in Table S5.

The thermodynamic analysis such as standard Gibbs free energy change (ΔG^o), the enthalpy change (ΔH^o) and entropy change (ΔS^o) were calculated for better understanding of the nature of adsorption behavior. The values of ΔH^o and ΔS^o can be calculated from the slope and intercept, respectively by plotting the values of lnK_d vs. 1/T (Figure S9). The thermodynamic parameters from the fitting line such as Gibbs free energy change ($G°$), the enthalpy change (ΔH^o), the entropy change (ΔS^o) and correlation coefficient (R^2) are listed in Table 1.

Table 1. Thermodynamic parameters for adsorption of cationic dyes (MB, RhB, MV) onto SiO_2NH_2-GO composite.

Dye	T(K)	ΔG° (KJ mol^{-1})	ΔH° (KJ mol^{-1})	ΔS° (KJ mol^{-1} K^{-1})	R^2
MB	298	-2.7	19.6	74.9	0.994
	313	-3.7			
	333	-5.3			
RhB	298	-0.3	52.6	177.1	0.992
	313	-2.4			
	333	-6.5			
MV	298	-1.4	38.8	112.9	0.997
	313	-3.0			

	333	-5.4

The negative values of ΔG^o determined at all of the experimental temperatures confirmed the spontaneous nature of the adsorption process. With the increasing temperature, the values of Gibbs free energy change (ΔG^o) become more negative indicating the increased adsorption capacity at equilibrium. The positive values of ΔH^o denote the endothermic nature of adsorption of cationic dyes onto SiO_2NH_2-GO composite. On the other hand, the positive values of ΔS^o shows the increment randomness at the surface of adsorbent during the adsorption process which can be reflected by the affinity of the SiO_2NH_2-GO for the cationic dyes.

3.5. Solid Phase Extraction (SPE) with SiO_2NH_2-GO

Currently exploited purification methods rely on time-consuming techniques usually generating problems including secondary pollutions or separation difficulties. Therefore, solid phase extraction process constitutes an attractive alternative for removal of contaminants such as cationic organic dyes. Due to the fast kinetics of adsorption process, the high saturation uptake capacity, the optimal pore size and high specific surface area as well as loose and powdery structure of obtained adsorbent we opted to apply the SiO_2NH_2-GO hybrid as solid phase extraction (SPE) column filling for rapid, effective and continuous adsorption of presented organic dyes. As the column was loaded with adsorbent, the filling was firstly activated with NaOH, to provide negative charge on the surface and enhance effectiveness of adsorption process. The uptake of the cationic dyes (MB, RhB and MV) from aqueous solutions was studied by using as-prepared SiO_2NH_2-GO material at the desired concentration and pH. The initial pH of solution can strongly affect the surface charge of adsorbent by dissociation of functional groups on active sites of GO as well as the ionization of organic dyes. To establish the adsorption mechanism, measurements of zero-point charge (pH_{pzc}) of the adsorbent are essential. The pH_{pzc} indicates the value of pH which refers to neutral charge of adsorbent and

constitutes one of the key factors for understanding the adsorption on carbon-based materials.[32, 74] The point of zero charge of SiO_2NH_2-GO corresponds to pH = 7.0 (Figure S10). Thus, at pH>7 ($pH>pH_{pzc}$), the surface charge of composite is negative. As a consequence, a significant adsorption process is observed at pH>7 because the electrostatic interactions between the cationic dyes and SiO_2NH_2-GO become stronger. Comparably the adsorption capacity of MB is almost ~5.2 times greater at pH=10 compared to acidic conditions. Notably, a dramatic difference is observed for MV, where basic conditions allow to increase the adsorption capacity even up to 33 times. The reusability of the column filling was conducted following the procedure described in previous section. The solid phase extraction experiments revealed that <99 % of MB, RhB and MV (Fig. S12) can be immediately adsorbed in just 3 min thereby highlighting the superior nature of SiO_2NH_2-GO composite with respect to most of graphene oxide-based adsorbents of organic dyes which typically requires long adsorption time, lower efficiency and separation problems (see Table S4 in Supporting Information).

The ability of the SiO_2NH_2-GO regeneration was determined in ten subsequent adsorption-desorption cycles, which is very important for its potential application. As presented on Figure S11, a decrease of about 7 % in the removal efficiency decreases of is observed after the first 2 cycles. Further experiments showed that each cycle causes a slight decrease of adsorption capacity, which might be explained by the collapsing of pores due to high volumetric flow of analyte over the experiments (~4L per cycle) resulting in lower pore volume after adsorption (Tab. S1). After 10 cycles the system is still able to adsorb from approx. 0.3 to 0.5 mmol of cationic dyes from aqueous solutions, which is more than 60% of initial adsorption capacity.

4. Conclusion

In summary, we have presented an easy and effective approach towards synthesis of SiO_2NH_2-GO composite, and its high efficiency for removal of cationic dyes from water. Various complementary characterization methods were employed to confirm the covalent attachment of

3-aminosilica-functionalized silica to GO. The novel porous material, with its high specific surface area (405.5 m^2 g^{-1}), exhibited high affinity toward cationic organic pollutants. The adsorption experiments show that cationic dyes (MB, RhB and MV) can be quantitatively adsorbed at pH 10 with maximum adsorption capacity as high as 300, 358 and 178 mg g^{-1}, respectively. The results proved superior performance of SiO_2NH_2-GO comparing to GO and aminosilica used for preparation of hybrid material. The adsorption mechanism of organic dyes on SiO_2NH_2-GO composite is ruled by the electrostatic interactions, however the planar structure of GO sheets favors the presence of π-π interactions, which further enhance the adsorption of MB, RhB and MV. The high maximum adsorption capacity as well as the time of adsorption provide much higher efficiency of dye removal than other GO-based sorbents of cationic organic dyes. Moreover, the obtained composite exhibited fast kinetics and was additionally efficiently investigated toward continuous adsorption as column filling. The presented system displayed excellent adsorption efficiency of ~99.7% for MB, RhB and MV in 3 min, high stability and reusability toward removal of cationic organic dyes paving the way to development silica-GO based materials of high-efficiency and low-cost water purification technologies.

Acknowledgements

This work was supported by the National Science Center (Grant No.2015/18/E/ST5/00188, and Grant No.2017/27/N/ST5/00173). Grant no. POWR.03.02.00-00-I026/16 co-financed by the European Union through the European Social Fund under the Operational Program Knowledge Education Development. The work was also supported by the European Commission through the Graphene Flagship Core 2 project (GA-785219) and the ERC project SUPRA2DMAT (GA-833707), as well as the Agence Nationale de la Recherche through the Labex project CSC (ANR-10-LABX-0026 CSC) within the Investissement d'Avenir program (ANR-10-120 IDEX-0002-02), and the International Center for Frontier Research in Chemistry (icFRC). D.

P. and S.W acknowledges the support from the Embassy of France in Poland in the form of a scholarship at the Institut de Science et d'Ingenierie Supramoleculaires, University of Strasbourg. Additionally, D.P acknowledge the support from Foundation for Polish Science (FNP) in the form of a scholarship.

Received: ((will be filled in by the editorial staff))
Revised: ((will be filled in by the editorial staff))
Published online: ((will be filled in by the editorial staff))

References

[1] P.J.J. Alvarez, C.K. Chan, M. Elimelech, N.J. Halas, D. Villagrán, Emerging opportunities for nanotechnology to enhance water security, Nat. Nanotech. 13(8) (2018) 634-641.
[2] S.M. Ghoreishi, R. Haghighi, Chemical catalytic reaction and biological oxidation for treatment of non-biodegradable textile effluent, Chem. Eng. J. 95(1) (2003) 163-169.
[3] H. Zollinger, Colour chemistry-synthesis, properties of organic dyes and pigments, VCH Publishers, New York, 1987.
[4] N. Buvaneswari, C. Kannan, Plant toxic and non-toxic nature of organic dyes through adsorption mechanism on cellulose surface, J. Hazard. Mater. 189(1) (2011) 294-300.
[5] Z. Aksu, Application of biosorption for the removal of organic pollutants: a review, Process Biochem. 40(3) (2005) 997-1026.
[6] U. Shanker, M. Rani, V.J.E.C.L. Jassal, Degradation of hazardous organic dyes in water by nanomaterials, Environ. Chem. Lett. 15(4) (2017) 623-642.
[7] C.-H. Weng, Y.-F. Pan, Adsorption of a cationic dye (methylene blue) onto spent activated clay, J. Hazard. Mater. 144(1) (2007) 355-362.
[8] M.A.M. Salleh, D.K. Mahmoud, W.A.W.A. Karim, A. Idris, Cationic and anionic dye adsorption by agricultural solid wastes: A comprehensive review, Desalination 280(1) (2011) 1-13.
[9] Y. Liu, F. Li, Q. Xia, J. Wu, J. Liu, M. Huang, J. Xie, Conductive 3D sponges for affordable and highly-efficient water purification, Nanoscale 10(10) (2018) 4771-4778.
[10] Y. Han, Z. Xu, C. Gao, Ultrathin graphene nanofiltration membrane for water purification, Adv. Funct. Mater. 23(29) (2013) 3693-3700.
[11] Q. Ma, Y. Yu, M. Sindoro, A.G. Fane, R. Wang, H. Zhang, Carbon-based functional materials derived from waste for water remediation and energy storage, Adv. Mater. 29(13) (2017) 1605361.
[12] I. Ali, New generation adsorbents for water treatment, Chem. Rev. 112(10) (2012) 5073-5091.
[13] W. Ma, J. Li, X. Tao, J. He, Y. Xu, J.C. Yu, J. Zhao, Efficient degradation of organic pollutants by using dioxygen activated by resin-exchanged iron(II) bipyridine under visible irradiation, Angew Chem Int Ed Engl 42(9) (2003) 1029-1032.
[14] A.V. Desai, B. Manna, A. Karmakar, A. Sahu, S.K. Ghosh, A water-stable cationic metal–organic framework as a dual adsorbent of oxoanion pollutants, Angew Chem Int Ed Engl 55(27) (2016) 7811-7815.

[15] P. Tan, J. Sun, Y. Hu, Z. Fang, Q. Bi, Y. Chen, J. Cheng, Adsorption of Cu2+, Cd2+ and Ni2+ from aqueous single metal solutions on graphene oxide membranes, J. Hazard. Mater. 297 (2015) 251-260.
[16] J. Ma, F. Yu, L. Zhou, L. Jin, M. Yang, J. Luan, Y. Tang, H. Fan, Z. Yuan, J. Chen, Enhanced adsorptive removal of methyl orange and methylene blue from aqueous solution by alkali-activated multiwalled carbon nanotubes, ACS Appl. Mater. Interfaces 4(11) (2012) 5749-5760.
[17] C.N.R. Rao, H.S.S. Ramakrishna Matte, U. Maitra, Graphene analogues of inorganic layered materials, Angew Chem Int Ed Engl 52(50) (2013) 13162-13185.
[18] K. Yang, J. Wang, B. Chen, Facile fabrication of stable monolayer and few-layer graphene nanosheets as superior sorbents for persistent aromatic pollutant management in water, J. Mater. Chem. A 2(43) (2014) 18219-18224.
[19] J. Wang, J. Hao, D. Liu, S. Qin, C. Chen, C. Yang, Y. Liu, T. Yang, Y. Fan, Y. Chen, W. Lei, Flower stamen-like porous boron carbon nitride nanoscrolls for water cleaning, Nanoscale 9(28) (2017) 9787-9791.
[20] S. Luo, X. Xu, G. Zhou, C. Liu, Y. Tang, Y. Liu, Amino siloxane oligomer-linked graphene oxide as an efficient adsorbent for removal of Pb(II) from wastewater, J. Hazard. Mater. 274 (2014) 145-155.
[21] K. Ai, C. Ruan, M. Shen, L. Lu, MoS2 nanosheets with widened interlayer spacing for high-efficiency removal of mercury in aquatic systems, Adv. Funct. Mater. 26(30) (2016) 5542-5549.
[22] D.R. Dreyer, A.D. Todd, C.W. Bielawski, Harnessing the chemistry of graphene oxide, Chem. Soc. Rev. 43(15) (2014) 5288-5301.
[23] V. Georgakilas, J.N. Tiwari, K.C. Kemp, J.A. Perman, A.B. Bourlinos, K.S. Kim, R. Zboril, Noncovalent functionalization of graphene and graphene oxide for energy materials, biosensing, catalytic, and biomedical applications, Chem. Rev. 116(9) (2016) 5464-5519.
[24] S. Eigler, A. Hirsch, Chemistry with Graphene and Graphene Oxide—Challenges for Synthetic Chemists, Angew. Chem. Int. Ed. 53(30) (2014) 7720-7738.
[25] V. Georgakilas, M. Otyepka, A.B. Bourlinos, V. Chandra, N. Kim, K.C. Kemp, P. Hobza, R. Zboril, K.S. Kim, Functionalization of graphene: covalent and non-covalent approaches, derivatives and applications, Chem. Rev. 112(11) (2012) 6156-6214.
[26] A.J. Fletcher, Y. Yüzak, K.M. Thomas, Adsorption and desorption kinetics for hydrophilic and hydrophobic vapors on activated carbon, Carbon 44(5) (2006) 989-1004.
[27] Z. Dong, D. Wang, X. Liu, X. Pei, L. Chen, J. Jin, Bio-inspired surface-functionalization of graphene oxide for the adsorption of organic dyes and heavy metal ions with a superhigh capacity, J. Mater. Chem. A 2(14) (2014) 5034-5040.
[28] Z. Cheng, J. Liao, B. He, F. Zhang, F. Zhang, X. Huang, L. Zhou, One-Step Fabrication of Graphene Oxide Enhanced Magnetic Composite Gel for Highly Efficient Dye Adsorption and Catalysis, ACS Sustain. Chem. Eng. 3(7) (2015) 1677-1685.
[29] M. Akrami, S. Danesh, M. Eftekhari, Comparative study on the removal of cationic dyes using different graphene oxide forms, J. Inorg. Org. Pol. Mater. 29(5) (2019) 1785.
[30] X. Zhang, D. Liu, L. Yang, L. Zhou, T. You, Self-assembled three-dimensional graphene-based materials for dye adsorption and catalysis, J. Mater. Chem. A 3(18) (2015) 10031-10037.
[31] K.C. Kemp, H. Seema, M. Saleh, N.H. Le, K. Mahesh, V. Chandra, K.S. Kim, Environmental applications using graphene composites: water remediation and gas adsorption, Nanoscale 5(8) (2013) 3149-3171.
[32] D. Pakulski, W. Czepa, S. Witomska, A. Aliprandi, P. Pawluć, V. Patroniak, A. Ciesielski, P. Samorì, Graphene oxide-branched polyethylenimine foams for efficient removal of toxic cations from water, J. Mater. Chem. A 6(20) (2018) 9384-9390.

[33] C. Anichini, W. Czepa, D. Pakulski, A. Aliprandi, A. Ciesielski, P. Samorì, Chemical sensing with 2D materials, Chem. Soc. Rev. 47(13) (2018) 4860-4908.
[34] R. Sitko, E. Turek, B. Zawisza, E. Malicka, E. Talik, J. Heimann, A. Gagor, B. Feist, R. Wrzalik, Adsorption of divalent metal ions from aqueous solutions using graphene oxide, Dalton Trans. 42(16) (2013) 5682-5689.
[35] F. Liu, S. Chung, G. Oh, T.S. Seo, Three-dimensional graphene oxide nanostructure for fast and efficient water-soluble dye removal, ACS Appl. Mater. Interfaces 4(2) (2012) 922-927.
[36] G.Z. Kyzas, E.A. Deliyanni, K.A. Matis, Graphene oxide and its application as an adsorbent for wastewater treatment, J. Chem. Technol. Biotechnol. 89(2) (2014) 196-205.
[37] M. Yusuf, F.M. Elfghi, S.A. Zaidi, E.C. Abdullah, M.A. Khan, Applications of graphene and its derivatives as an adsorbent for heavy metal and dye removal: a systematic and comprehensive overview, RSC Adv. 5(62) (2015) 50392-50420.
[38] G.K. Ramesha, A. Vijaya Kumara, H.B. Muralidhara, S. Sampath, Graphene and graphene oxide as effective adsorbents toward anionic and cationic dyes, J. Colloid Interface Sci. 361(1) (2011) 270-277.
[39] Y. Shen, Q. Fang, B. Chen, Environmental Applications of Three-Dimensional Graphene-Based Macrostructures: Adsorption, Transformation, and Detection, Environmental Science & Technology 49(1) (2015) 67-84.
[40] C.T. Kresge, M.E. Leonowicz, W.J. Roth, J.C. Vartuli, J.S. Beck, Ordered mesoporous molecular sieves synthesized by a liquid-crystal template mechanism, Nature 359(6397) (1992) 710-712.
[41] Z. Wu, D. Zhao, Ordered mesoporous materials as adsorbents, Chem. Commun. 47(12) (2011) 3332-3338.
[42] C.T. Kresge, M.E. Leonowicz, W.J. Roth, J.C. Vartuli, J.S. Beck, Ordered mesoporous molecular sieves synthesized by a liquid-crystal template mechanism, Nature 359 (1992) 710.
[43] P.N.E. Diagboya, E.D. Dikio, Silica-based mesoporous materials; emerging designer adsorbents for aqueous pollutants removal and water treatment, Microporous Mesoporous Mater. 266 (2018) 252-267.
[44] Y.-W. Chen, P.-J. Chen, S.-H. Hu, I.-W. Chen, S.-Y. Chen, NIR-Triggered Synergic Photo-chemothermal Therapy Delivered by Reduced Graphene Oxide/Carbon/Mesoporous Silica Nanocookies, Adv. Funct. Mater. 24(4) (2014) 451-459.
[45] S. Sreejith, X. Ma, Y. Zhao, Graphene Oxide Wrapping on Squaraine-Loaded Mesoporous Silica Nanoparticles for Bioimaging, J. Am. Chem. Soc. 134(42) (2012) 17346-17349.
[46] S. Yang, X. Feng, L. Wang, K. Tang, J. Maier, K. Müllen, Graphene-Based Nanosheets with a Sandwich Structure, Angew Chem Int Ed Engl 49(28) (2010) 4795-4799.
[47] X. Liu, H. Zhang, Y. Ma, X. Wu, L. Meng, Y. Guo, G. Yu, Y. Liu, Graphene-coated silica as a highly efficient sorbent for residual organophosphorus pesticides in water, J. Mat. Chem. A 1(5) (2013) 1875-1884.
[48] R. Sitko, B. Zawisza, E. Talik, P. Janik, G. Osoba, B. Feist, E. Malicka, Spherical silica particles decorated with graphene oxide nanosheets as a new sorbent in inorganic trace analysis, Anal. Chim. Acta 834 (2014) 22-29.
[49] Q. Liu, J.B. Shi, J.T. Sun, T. Wang, L.X. Zeng, G.B. Jiang, Graphene and Graphene Oxide Sheets Supported on Silica as Versatile and High-Performance Adsorbents for Solid-Phase Extraction, Angew. Chem.-Int. Edit. 50(26) (2011) 5913-5917.
[50] S.O. Akpotu, B. Moodley, Encapsulation of Silica Nanotubes from Elephant Grass with Graphene Oxide/Reduced Graphene Oxide and Its Application in Remediation of Sulfamethoxazole from Aqueous Media, ACS Sustain. Chem. Eng. 6(4) (2018) 4539-4548.

[51] A.S. Krishna Kumar, S.-J. Jiang, W.-L. Tseng, Facile synthesis and characterization of thiol-functionalized graphene oxide as effective adsorbent for Hg(II), J. Environ. Chem. Eng. 4(2) (2016) 2052-2065.
[52] A. Meng, J. Xing, Z. Li, Q. Li, Cr-doped ZnO nanoparticles: synthesis, characterization, adsorption property, and recyclability, ACS Appl. Mater. Interfaces 7(49) (2015) 27449-27457.
[53] S. Chakraborty, S. Saha, V.R. Dhanak, K. Biswas, M. Barbezat, G.P. Terrasi, A.K. Chakraborty, High yield synthesis of amine functionalized graphene oxide and its surface properties, RSC Adv. 6(72) (2016) 67916-67924.
[54] A.C. Ferrari, J.C. Meyer, V. Scardaci, C. Casiraghi, M. Lazzeri, F. Mauri, S. Piscanec, D. Jiang, K.S. Novoselov, S. Roth, A.K. Geim, Raman spectrum of graphene and graphene layers, Phys. Rev. Lett. 97(18) (2006) 187401.
[55] D. Zhou, B.-H. Han, Graphene-based nanoporous materials assembled by mediation of polyoxometalate nanoparticles, Adv. Funct. Mater. 20(16) (2010) 2717-2722.
[56] W. Li, X.-Z. Tang, H.-B. Zhang, Z.-G. Jiang, Z.-Z. Yu, X.-S. Du, Y.-W. Mai, Simultaneous surface functionalization and reduction of graphene oxide with octadecylamine for electrically conductive polystyrene composites, Carbon 49(14) (2011) 4724-4730.
[57] M.M. Lucchese, F. Stavale, E.H.M. Ferreira, C. Vilani, M.V.O. Moutinho, R.B. Capaz, C.A. Achete, A. Jorio, Quantifying ion-induced defects and Raman relaxation length in graphene, Carbon 48(5) (2010) 1592-1597.
[58] K. Krishnamoorthy, M. Veerapandian, K. Yun, S.J. Kim, The chemical and structural analysis of graphene oxide with different degrees of oxidation, Carbon 53 (2013) 38-49.
[59] Y. Xu, H. Bai, G. Lu, C. Li, G. Shi, Flexible graphene films via the filtration of water-soluble noncovalent functionalized graphene sheets, J. Am. Chem. Soc. 130(18) (2008) 5856-5857.
[60] X. Zhang, Y. Huang, Y. Wang, Y. Ma, Z. Liu, Y. Chen, Synthesis and characterization of a graphene–C60 hybrid material, Carbon 47(1) (2009) 334-337.
[61] R.J. Hunter, Zeta potential in colloid science: principles and applications, Academic Press; 2013.
[62] H. Wang, X. Zhou, Q. Chen, Removal of cationic dyes from aqueous solution using carbon-encapsulated superparamagnetic colloidal nanoparticles as adsorbent, Nano 8(1) (2013) 1350006.
[63] S. Wang, Z.H. Zhu, Effects of acidic treatment of activated carbons on dye adsorption, Dyes Pigm. 75(2) (2007) 306-314.
[64] J.R. Kim, B. Santiano, H. Kim, E. Kan, Heterogeneous oxidation of methylene blue with surface-modified iron-amended activated carbon, Am. J. Anal. Chem. 4(7A) (2013) 8.
[65] P. Wang, M. Cheng, Z. Zhang, On different photodecomposition behaviors of rhodamine B on laponite and montmorillonite clay under visible light irradiation, J. Saudi Chem. Soc. 18(4) (2014) 308-316.
[66] Y.-R. Zhang, S.-Q. Wang, S.-L. Shen, B.-X. Zhao, A novel water treatment magnetic nanomaterial for removal of anionic and cationic dyes under severe condition, Chem. Eng. J. 233 (2013) 258-264.
[67] Y. Qi, M. Yang, W. Xu, S. He, Y. Men, Natural polysaccharides-modified graphene oxide for adsorption of organic dyes from aqueous solutions, J. Colloid Interface Sci. 486 (2017) 84-96.
[68] B.M. Lowe, C.-K. Skylaris, N.G. Green, Acid-base dissociation mechanisms and energetics at the silica–water interface: An activationless process, J. ColIoid Interface Sci. 451 (2015) 231-244.
[69] Z. Pei, L. Li, L. Sun, S. Zhang, X.-q. Shan, S. Yang, B. Wen, Adsorption characteristics of 1,2,4-trichlorobenzene, 2,4,6-trichlorophenol, 2-naphthol and naphthalene on graphene and graphene oxide, Carbon 51 (2013) 156-163.

[70] J. Xu, L. Wang, Y. Zhu, Decontamination of bisphenol a from aqueous solution by graphene adsorption, Langmuir 28(22) (2012) 8418-8425.
[71] S. Nayab, A. Farrukh, Z. Oluz, E. Tuncel, S.R. Tariq, H.u. Rahman, K. Kirchhoff, H. Duran, B. Yameen, Design and fabrication of branched polyamine functionalized mesoporous silica: an efficient absorbent for water remediation, ACS Appl. Mater. Interfaces 6(6) (2014) 4408-4417.
[72] S. Ghorai, A.K. Sarkar, A.B. Panda, S. Pal, Effective removal of Congo red dye from aqueous solution using modified xanthan gum/silica hybrid nanocomposite as adsorbent, Biores. Technol. 144 (2013) 485-491.
[73] J. Rahchamani, H.Z. Mousavi, M. Behzad, Adsorption of methyl violet from aqueous solution by polyacrylamide as an adsorbent: Isotherm and kinetic studies, Desalination 267(2) (2011) 256-260.
[74] A.S.K. Kumar, S.-J. Jiang, Chitosan-functionalized graphene oxide: A novel adsorbent an efficient adsorption of arsenic from aqueous solution, J. Environ. Chem. Eng. 4(2) (2016) 1698-1713.